 doi:10.20944/preprints202101.0336.v1

Article

Achieving Ultra-High Performance Concrete by using packaging models in combination with nanoadditions

J. Díaz[1,2], J.C. Gálvez[1*], M. G. Alberti[1], A. Enfedaque[1]

[1] Departamento de Ingeniería Civil: Construcción, E.T.S de Ingenieros de Caminos, Canales y Puertos, Universidad Politécnica de Madrid. C / Profesor Aranguren, s/n, 28040, Madrid.; e-mail@e-mail.com
[2] Lantania C/Sobrado, 2, 28050, Madrid; e-mail@e-mail.com
* e-mail: jaime.galvez@upm.es phone: +34 910 674 125

Abstract: This paper describes the packaging models that are fundamental for the design of ultra-high-performance concrete (UHPC), and their evolution. They are divided into two large groups: continuous and discrete models. The latter are those that provide the best answer in obtaining an adequate simulation of the packing of the particles up to nanometric size. This includes the interaction among the particles by means of loosening and wall coefficients, allowing a simulation of the virtual and real compactness of such particles. In addition, a relationship between virtual and real compactness is obtained, through the compaction index, which may simulate the energy of compaction that the particles undergo in their placement in the mold. The use of last-generation additives allows such models to be implemented with water-cement (w/c) ratios close to 0.18. However, the premise of maximum packing as a basic pillar for the production of UHPC should not be the only one. The cement hydration process affected by nanoadditions and the ensuing effectiveness in the properties in both fresh and hardened state according to the respective percentages in the mixture should also be studied. An adequate ratio and proportion of these additions may lead to an obtaining of better results even with lower levels of compactness.

Keywords: Particle packing, packaging models, packaging density, concrete, addition, nano addition, ultra-high-performance concrete.

1. Introduction

In the design of ultra-high-performance concrete (UHPC), the so-called "minimum defect" is established as the main objective. Such an objective entails creating a material with the minimum number of voids (micro-cracks and interconnected pores) in order to reach the potential resistance of the components and increasing the durability of the concrete. For this reason, an optimisation of the packing of particles is established in the design by means of models that consider the individual compactness of each component and the maximum compactness obtained by the set of components. However, this maximum compactness, which is translated into mixing percentages, may not always be the most optimal in terms of hydration of paste and resistance. Therefore, this study seeks to balance the maximum compactness obtained by means of packaging models with the optimum ratio among the materials and by considering hydration processes. Additions, such as nanosilica or metakaolin, favour the formation of calcium silicate hydrate (C-S-H) which allows an improvement in strength and durability by reducing the porous network, though the percentages should be limited to certain values in order to achieve a greater degree of effectiveness [8, 44].

According to the ACI Committee 239 and also the Federal Highway Adminitration (FHWA) [1], UHPC is a concrete with at least 150 MPa of compressive strength. Other definitions refer to compressive strength of at least 120 MPa. In this material, composed

Preprints (www.preprints.org) | NOT PEER-REVIEWED | Posted: 18 January 2021 doi:10.20944/preprints202101.0336.v1

of a cement paste, aggregates and additions with a high level of packing, coarse aggregates are not usually utilised (the maximum size is usually between 150-600 μm). Although with the increase of experience and optimisation in the densification of the design aggregates with a maximum size larger than 8 mm have been included (especially basaltic and quartzite aggregates) [2]. The water/cement (*w*/*c*) ratios are lower than 0.25, having been obtained through use of high-effectiveness additives that confer self-compacting concrete rheological properties.

Therefore, the significance of this research entails consideration of combining packaging models, focussing on physical optimisation of components with the optimal percentages and - from the chemical point of view- inclusion of nanoadditions that allow the best results both in terms of resistance and of durability.

2. Packaging models

The priorities in the design of UHPC involve obtaining high density and packing of particles. The high degree of compactness of the fine particles reduces the demand for water for the same workability, thus obtaining a decrease in the water/fine (*w*/*f*) ratio [3]. The range of UHPC concrete considers use of additions and nanomaterials, such as silica fume, fly ash, microsilica and metacaolin with sizes of 120 nm or nanosilica with maximum size of 5 nm. The specific surface area (SSA) is inversely proportional to the particle size. The high specific surface area and the size of these materials allow them to occupy the interstices between the cementitious paste and the aggregate, thus favouring packaging.

In 1616, Kepler showed that in an ordered hexagonal sphere closure (HCP) of the same diameter the theoretical maximum packing is 74.05% $\left(\frac{\pi}{3\cdot\sqrt{2}}\right)$, which is the same value for a face-centred cubic (FCC) structure. For a HCP structure, and with random packing, this would be 64% for spheres of the same diameter [4].

Hence, in order to increase the packing level, it is necessary to use spheres of lower diameters capable of filling the uncovered voids [21, 2]. Horsfield established the maximum packing rates for five different particles for the hexagonal close [5].

Table 1 Horsfield model of packing.

Sphere (nº)	Relative diameter	Packing (%)
1	1	74.0
2	0.414	79.3
3	0.225	81.0
4	0.177	84.2
5	0.116	85.1

Packaging methods can be divided into two groups: continuous and discrete (binary or multicomponent) with or without interaction. The first one is based on the creation of a continuous particle size curve, using decreasing particle sizes. There are several models referred to as continuous. Initial models such as those provided by Fuller and Thompson (1907), involve a theoretical curve being established that relates the maximum size of the aggregate (*D*) and the sieve of the series used (*d*), with the variant of Gessner looking for a parabola [6].

$$y(d) = \left(\frac{d}{D}\right)^r \quad (1)$$

Preprints (www.preprints.org) | NOT PEER-REVIEWED | Posted: 18 January 2021 doi:10.20944/preprints202101.0336.v1

The Andreasen and Andersen model (A&A, A&A M) [7] changes the parameter of the Gessner parabola from r=0.5 to r=0.33-0.5 to obtain a higher degree of packing. In UHPC, a good packing level has been obtained with values of r=0.23 [8]. The Fuller and Thompson model, modified by Gessner, does not establish an adequate densification for materials with particles lower than 250 μm, obtaining mixtures that are poor in cement content [9]. Conversely, the aforementioned A&A model establishes a curve up to the zero value, with it not being limited to a minimum necessary particle size (*Dmin*). The modification of the A&A model (A&A M) established by Funk and Dinger [23] introduces the graduation of the curve and considers the minimum particle size (see Figure 1).

$$y(d) = \left(\frac{d^r - D_{min}^r}{D^r - D_{min}^r}\right) \quad (2)$$

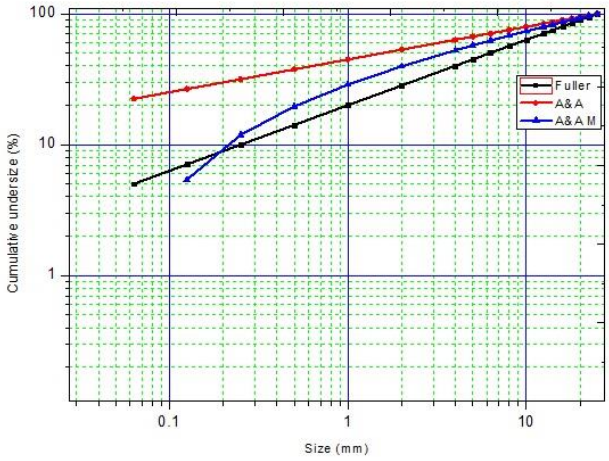

Figure 1. Particle size distributions: Fuller, A&A, A&A M *D*=25 mm, *Dmin*=63μm.

However, the aforementioned models are not always adapted to real systems, given that the particle size continuity of each component to be mixed is not guaranteed. The optimum packaging level for a UHPC concrete is not always reached, although the modification of the A&A method has been used in research for the manufacture of UHPC and ultra-high-performance and fibre-reinforced concrete (UHPFRC) [8, 10]. These limitations can be addressed with the second group of packaging models, that is to say, discrete packaging models. This entails establishing particle systems where at least one is dominant and which guarantees the solid continuity of the granular body [11]. The rest of the particles are packaged around the skeleton of the dominant class [21].

The first discrete packaging model, valid for spheres, was Furnas' binary model (1929) which (a year later) Westman and Hugill applied to multicomponent models [12, 21, 13]. In both models there are two conditions: the first is that there is no interaction between the particles, and the second is that some particles enter the gaps left by the other particles. Furnas initially related the void index of the mixture (ε), with the void index of the components (ε_1, ε_2) and the volume fraction of component 1 in the mixture (S_{v1}). By choosing the higher value of the expressions (3) and (4), this may be better understood through examination of Figure 2.

$$\varepsilon = 1 - \frac{1 - \varepsilon_1}{S_{v1}} \quad (3)$$

$$\varepsilon = 1 - \frac{1 - \varepsilon_2}{1 - S_{v1}\varepsilon_2} \quad (4)$$

Preprints (www.preprints.org) | NOT PEER-REVIEWED | Posted: 18 January 2021 doi:10.20944/preprints202101.0336.v1

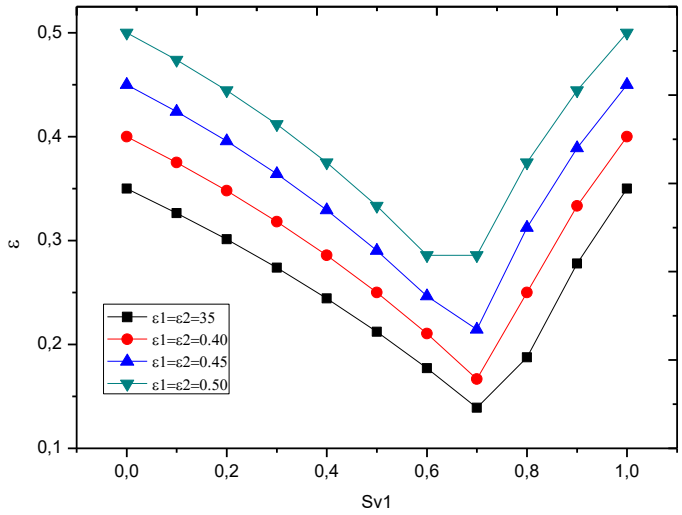

Figure 2. Void fraction for various fractions of component 1.

Westman and Hugill identified (see Figure 3) the apparent volume *Va*, inverse of compactness "*c*", as the volume necessary to obtain an absolute volume equal to unity, establishing a pore index "*e*" that meets *Va=e+1=1/c*, with *a1* and *a2* being the apparent volumes of the coarse and fine particles respectively and "*y1*", "*y2*" the volume fractions of each class. In Figure 3 the lines "*a*" and "*b*" are represented, respectively, as the absolute volumes of the coarse and fine particles. It should also be noted that lines "*e*" and "*d*" denote, respectively, the apparent volumes of the fine and coarse particles. Line "*c*" represents the sum of absolute volumes of all particles equal to value one. Line "*f*" represents the binary mixture, establishing a turning point when the void index is lower and compactness is at a maximum. This line is composed of line "*d*" for coarse particles and line "*f'*. Therefore, should the mixture the coarse particles be dominant, expression (5) would be obtained and for mixtures with dominant fine particles, expression (6). The best mixture corresponds to the highest value of both such expressions or the lowest value of expressions (9) and (10), where "*c*" is the compactness. Where $\alpha 1$ y $\alpha 2$ correspond to the real compactness of each class, Φ_1 and Φ_2 are the volumes occupied by each class in the mixed volume.

$$v_{a1}=a_1y_1=y_1/\alpha_1=(1-y_2)(1+e_1) \tag{5}$$

$$v_{a2}=y_1+a_2y_2=y_1+y_2/\alpha_2=1+e_2y_2 \tag{6}$$

$$y_1=\frac{\Phi_1}{\Phi_1+\Phi_2} \tag{7}$$

$$y_2=\frac{\Phi_2}{\Phi_1+\Phi_2} \tag{8}$$

$$c_1=\alpha_1+\Phi_2=\frac{\alpha_1}{y_1}=\frac{\alpha_2}{1-y_2} \tag{9}$$

$$c_2=\alpha_2+(1-\alpha_2)\Phi_1=\frac{\alpha_2}{1-(1-\alpha_2)y_1} \tag{10}$$

Preprints (www.preprints.org) | NOT PEER-REVIEWED | Posted: 18 January 2021 doi:10.20944/preprints202101.0336.v1

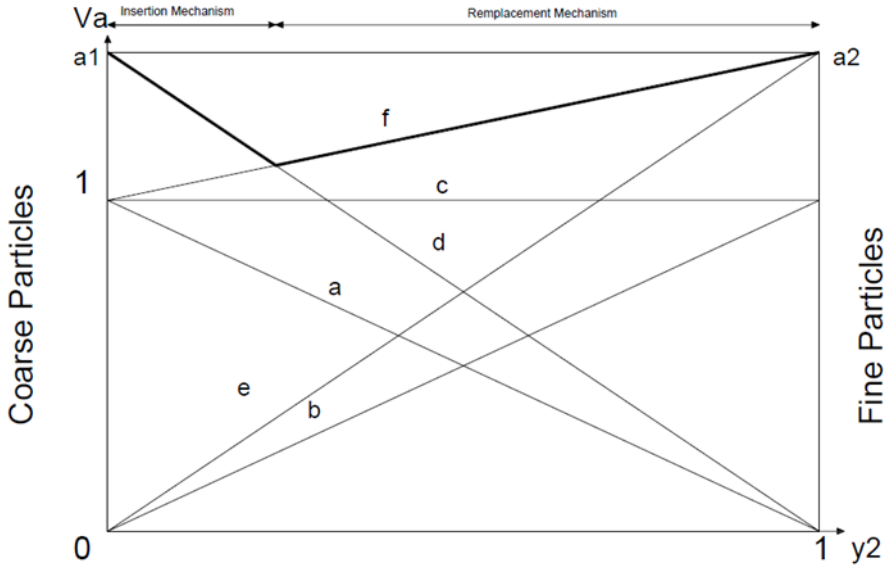

Figure 3. Evolution of bulk volume in binary mixture as a function of the proportion of fine particles, Westman and Hugill model [14].

Authors such as Ben-Aïm [22] (1970), Sotovall *et al*.[23], De Larrard *et al*.[26] (1986) examined the two most important restrictions to packing. Another study, which entailed proposing the wall and loosening effect, was provided by Caquot in 1937. The wall effect occurs when the predominant fines or container displace them locally. The loosening effect takes place when the size of the fines is greater than the voids they occupy, distancing the thicknesses. The relationship between particle size (*d1/d2*) is fundamental to these effects.

Sotovall and De Larrard, also based on Mooney's model (1950) for predicting the viscosity of monodisperse particle suspensions in a liquid medium, obtained a method of packing by searching for the proportion necessary to obtain an infinite viscosity. They named it the linear packing density model (LPDM) [15], where the wall effect and loosening interactions were established. However, given that it is not possible to represent the random behaviour of the real packing, the solid suspension model (SSM) was established later where viscosity is delimited to finite (introducing the interactions between virtual and real compactness).

In the LPDM model, as shown in expression (11), the packing of a "*t*" particle is established and considers the loosening and wall effects. Thus, expressions (12) and (13) represent the loosening and wall effects, respectively, of the mixture and depending on the binary relations or interactions between the particle sizes (*z; d1/d2*). Where *y(t)* is the volume fraction of size "*t*" in the mixture, and taking into account the expression (14) ($\int_d^D \boldsymbol{y(x)dx} = \mathbf{1}$), where *d* and *D* are the minimum and maximum particle size, respectively, $\beta(t)$ is the virtual packing density and $\alpha(t)$ is the real packing density.

In the SSM model, the starting point is Mooney's viscosity model [24] which relates the solid content ϕ, ordered at random, and the relative viscosity ηr according to the expression (17) (a model used again by several researchers from the 1980s onwards with the advance of additives and the need to link workability and compactness). Thus, taking the HCP structure as an example, where the packing density of the ordered spheres is 0.74 and such density of the unordered form is 0.64, a relative viscosity of ηr =1.36*105 may be

Preprints (www.preprints.org) | NOT PEER-REVIEWED | Posted: 18 January 2021 doi:10.20944/preprints202101.0336.v1

obtained, called reference viscosity ηr^{ref}. Expression (16) establishes the variation of viscosity ηr, for a particle size of "t", between D and d, depending on the virtual $\beta(t)$ and real packing $\alpha(t)$.

Expression (15) establishes the virtual packing density $\beta(t)$ as a function of the real packing $\alpha(t)$ through the adapted expression (16) of Mooney's viscosity. Expression (17) represents the ratio of "yi" volumetric fractions and virtual packing in a system, no longer binary but N particles.

$$c(t) = \frac{\alpha(t)}{1 - \int_{Dmin}^{t} y(x) f\left(\frac{x}{t}\right) dx - [1 - \alpha(t)] \cdot \int_{t}^{D} y(x) g\left(\frac{t}{x}\right) dx}; \tag{11}$$

$$c = \min\big(c(t)\big);\ y(t) > 0$$

$$f(z) = 0.7(1 - z) + 0.3\,(1 - z)^{12} \tag{12}$$

$$g(z) = (1 - z)^{1.3} \tag{13}$$

$$\int_{d}^{D} y(x)dx = 1 \tag{14}$$

$$c(t) = \frac{\beta(t)}{1 - \int_{d}^{t} y(x) f\left(\frac{x}{t}\right) dx - [1 - \beta(t)] \cdot \int_{t}^{D} y(x) g\left(\frac{t}{x}\right) dx} \tag{15}$$

$$\eta_r^{ref} = \exp\left(\frac{2.5}{\frac{1}{\alpha(t)} - \frac{1}{\beta(t)}}\right);\ d \le t \le D;\ \eta_r^{ref} = \exp \int_{d}^{D} \left(\frac{2.5 \cdot y(t)}{\frac{1}{c} - \frac{1}{c(t)}}\right); \tag{16}$$

$$\eta_r = \exp\left(\frac{2.5}{\frac{1}{\Phi} - \frac{1}{\beta}}\right) = \eta_r^{ref}$$

HCP: Φ=0.64; β=0.74; η_r^{ref}=1.36*10^5

$$\frac{1}{\beta(t)} = \sum_{1}^{N} \frac{y_i(t) = 1}{\beta_i(t)} \tag{17}$$

Yu and Standish [25] (1987) developed a model like that provided Sotovall *et al*.from the initial model offered by Westman.

In 1999, De Larrard *et al*. developed the compressible packaging model (MEC) which introduces the compaction index K, representative of the energy supplied in the compaction and the type of stacking, that is to say, the process of building the stack. This led to a third-generation model being established where, in addition to taking into account the

Preprints (www.preprints.org) | NOT PEER-REVIEWED | Posted: 18 January 2021 doi:10.20944/preprints202101.0336.v1

real and virtual packing of the mixtures, it introduced packing levels as a function of the compacting energy of the relationship between both packaging densities [14].

This model establishes the calculation of the virtual compactness γ based on the characteristics of each particle type in an ordered mixture, proportion yi and unit virtual compactness βi. Subsequently, the method calculates the real compactness ϕ (αi of each particle) ordered randomly. The compaction index K relates each compact, the real compactness of the mixture ϕ grows with the value of K. Thus, for each K index, a real maximum compactness ϕ determined in the mixture will be obtained.

For the general case with interaction in polydisperse system, the MEC starts from a ternary mixture, where the dominant class with grain size $d2$ suffers the effect of loosening, aij, by the class with grain size $d3$, with $d2>d3$ and the wall effect, bij, by the grain class d1 with $d1>d2$. Expression (18) establishes the virtual compactness of a mixture where class i is dominant.

$$\gamma_i = \frac{\beta_i}{1 - \sum_{j=1}^{i-1}\left[1 - \beta_i + b_{ij}\beta_i(1 - \frac{1}{\beta_j})\right]y_j - \sum_{j=i+1}^{n}\left[1 - a_{ij}\beta_i/\beta_j\right]y_j} \tag{18}$$

Then real compactness is established. As indicated in previous points, the real compactness ϕ responds to a packing of the particles by means of a determined compacting method. By establishing that $\phi<\gamma$, the method identifies a relationship between virtual and real packing, through the compaction index K. An increasing of the efficiency of the compaction method leads to a subsequent increase in real compactness. Each compaction method (discharge, crushing, vibration, vibration + pressure, as shown in Table 2) has a specific value of K [14, 27] and the expression (20). The compaction index of grain class "i", Ki, will be related to the actual compactness (volume of the solid), ϕi, that grain class and to the maximum actual compactness (volume of the solid), ϕi^*,which that grain class "i" will have in the presence of other grain classes. When class "i" is dominant in the mixture $\phi i^*=\phi i$ ($K=\infty$), the H function takes values between 0 and 1, ratio variation $\phi i/\phi i^*$ (20), exhibiting a trend to the zero value for the minimum compaction index and to the value one when the compaction index is maximum ($K=\infty$). In expression (22) the compaction index is established as the relationship between the known fractions of each class yi, the compactness βi, γi and the real compactness of the mixture. Implicit expression in K, given that the rest of parameters are known or calculated according to their placement, proportion and interaction [27]. According to expression (22), for each compactness value ϕ there is a value of K. For a packing of particles of the same size, expression (23) would be obtained which is implicit in βi.

$$K = \sum_{i=1}^{n} K_i \tag{19}$$

$$K_i = H\left(\frac{\Phi_i}{\Phi_i^*}\right) \tag{20}$$

$$K = \sum_{i=1}^{n}\left(\frac{\frac{\Phi_i}{\Phi_i^*}}{1 - \frac{\Phi_i}{\Phi_i^*}}\right) \tag{21}$$

Preprints (www.preprints.org) | NOT PEER-REVIEWED | Posted: 18 January 2021 doi:10.20944/preprints202101.0336.v1

$$K = \sum_{i=1}^{n} K_i = \sum_{i=1}^{n} \frac{{}^{y_i}/_{\beta_i}}{\frac{1}{\Phi} - \frac{1}{\gamma_i}} \quad (22)$$

$$K = \frac{1}{\frac{\beta_i}{\Phi_i} - 1};\ \beta_i = \frac{1+K}{K} \cdot \Phi_i \quad (23)$$

Tabla 2 Compaction rates by type of packing

Type of packaging	Packing mode	*K*
Dry packing	Simple stacking	4.1
	Manual compaction with bar	4.5
	Vibration	4.75
	Vibration + pressure (10 KPa)	9
Wet packing	Water demand	6.7
Virtual packing		$\propto$

The first approximation to the wall effect was made by Caquot in 1937, indicating that the reduction of compactness of the smaller grains with size *d2* around the thicker grains with size *d1* results in a variation of volume proportional to the surface of the interface [14]. Caquot identified a linear relationship between 0 and 1 for the wall coefficient, $b12=x$; ($x=d2/d1$). Authors such as the aforementioned Ben Aïm established a disturbance zone in the contact between coarse and fine particles where a reduction in compactness occurred, depending on the level of insertion of the fine grains in the disturbance zone, an approximation that can be established is $b12=2x$. Therefore, for grain sizes with $d1=d2$ the wall coefficient does not tend to the value one. Dodds provided a model for calculating the wall coefficient based on the theoretical model of hexagonal-close packing (HCP), with $\beta=0.74$, where the tendency of the wall effect for $d1=d2$ tends to the value of one, obtaining values greater than one for values of x between $0.6<x<1$. However, this model establishes a maximum packing, something that does not occur in reality and with the voids left being filled by particles that also meet the condition of full contact. The function that represents the wall coefficient indicated in the MLC was obtained empirically by means of the previously mentioned theoretical models, expression (24) represents the wall coefficient of the MLC. This function was later adjusted until expression (25) was obtained in the MEC. Figure 4 represents the function of the wall effect coefficient, tending to value one for $d1=d2$.

$$b(x) = 1 - (1-x)^{1.6} \quad (24)$$

$$b(x) = 1 - (1-x)^{1.5} \quad (25)$$

Preprints (www.preprints.org) | NOT PEER-REVIEWED | Posted: 18 January 2021 doi:10.20944/preprints202101.0336.v1

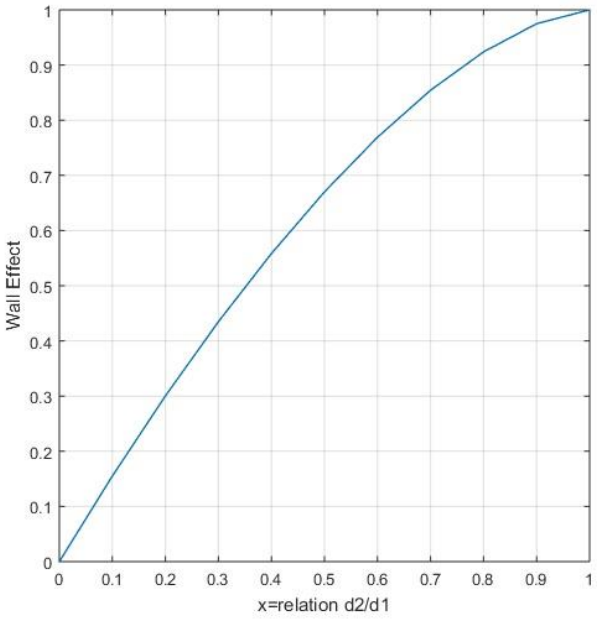

Figure 4. Wall effect function in MEC.

In the MLC model, Sotovall [23] offers a hypotheses to establish the alienation effect in a binary mixture. It first indicates that the void left in space (3D) by four contacting spheres of diameter *d1* may be occupied by a sphere of diameter *d2*. That, in turn, will be tangent to the rest of the spheres and therefore will not cause separation or a reduction in compactness. The critical diameter ratio, between the spheres of different diameters, would be *x0=0.224* (*x≈0.2*), (*x0=0.154* for three spheres in one plane) as depicted in Figure 5. It also shows that the insertion of spheres with a diameter *d2* greater than the value $\boldsymbol{x_0 \cdot d_1}$ leads to a decrease in the point compactness of particles with a diameter *d1*, form *β1* to *β'1*. The voids left will be filled with small particles whose proportion *β** is linearly related to the ratio of diameters *x*. In addition, when *x→1*, compactness with dominant fines or coarse is equal and their volume fraction is equal to 0.5.

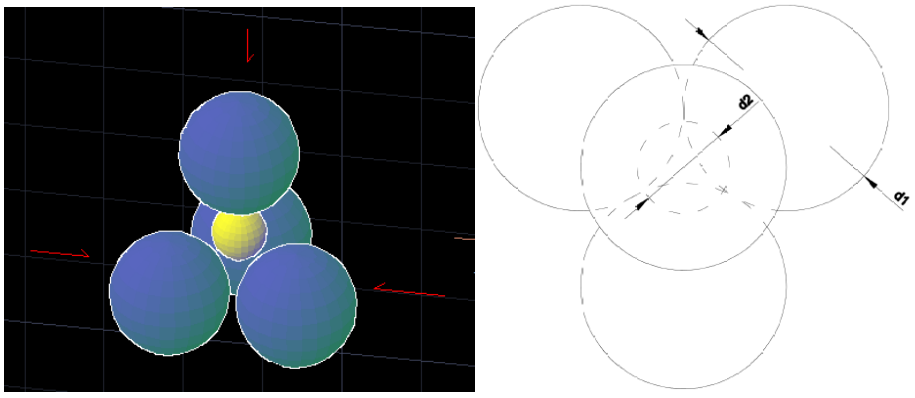

(a) *(b)*

Figure 5. Packing of four spheres with diameter d_1 and $d_2=0.224d_1$.

The loosening function embodied in the MLC is set out in the following expressions, indicating that for a lower ratio of *x0<0.2* the value of the coefficient is zero. Figure 6 represents the function of expression (26), for random packing (*β=0.64*) and HCP (*β=0.74*),

Preprints (www.preprints.org) | NOT PEER-REVIEWED | Posted: 18 January 2021 doi:10.20944/preprints202101.0336.v1

establishing an upper limit of 1 and a considerable increase in the distance coefficient between *0.2<x<0.3*.

$$a(x) = \frac{\left(1 - \left({}^{x_0}/_{x}\right)^3\right)}{(1 - x_0^3) \cdot \left((1 - \beta - \frac{3x_0^3}{1 - x_0^3}(1 - x) + 1\right) \cdot} \qquad x \geq x_0 \quad (26)$$

$$a(x) = 0 \qquad x < x_0 \quad (27)$$

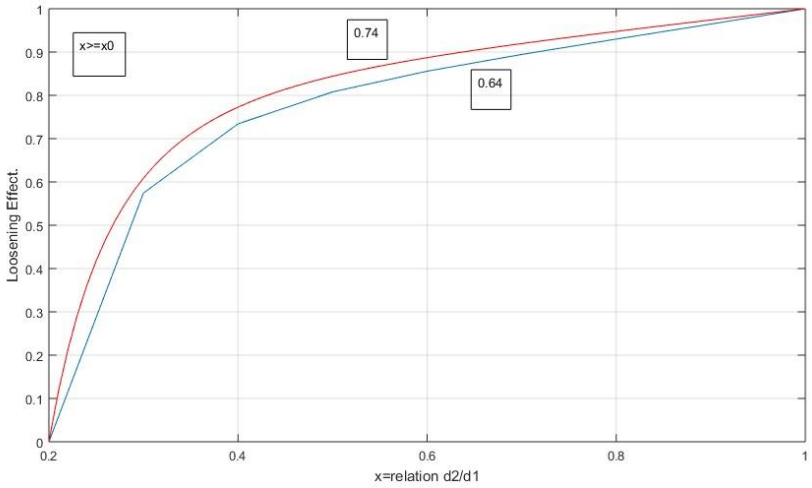

Figure 6. Loosening coefficient function in MLC.

Larrrard [14, 26, 27] provided a function of the loosening coefficient according to empirical measurements. In this case, the hypothesis of *a(0)=0* and *a(1)=1* is maintained, though no null value is established for diameter ratios of less than 0.2, as indicated by Sotovall (though the horizontal tangent is established at 1 and 0). Expression (28) shows the function of the loosening coefficient proposed by Larrad. Other authors, such as Yu *et al*., established a function of the loosening coefficient with higher values for lower size ratios [14, 28], with a similar trend to that indicated by De Larrard. The expressions (28) and (29) establish, respectively, the functions of De Larrard and Yu.

In later research, Sotovall *et al*.[14] carried out empirical studies on samples of rolled and crushed aggregates, identifying a new function of the loosening coefficient indicated in expression (30). It should be noted that there is no horizontal tangent at 1 and a vertical tangent is established at 0, and that the values of a (0) and a (1), continue to prevail. This function was modified for other experimental cases provided by Lecomte *et al*, as shown in expression (31). Lastly, in the De Larrard SCM method, a new function was established for the loosening coefficient, indicated in expression (32). Figure 7 shows the functions of the loosening coefficient according to the studies.

$$a(x) = 1 - (1 - x)^{3.1} - 3.1 \cdot x \cdot (1 - x)^{2.9} \quad (28)$$

$$a(x) = 1 - (1 - x)^{3.33} - 2.81 \cdot x \cdot (1 - x)^{2.77} \quad (29)$$

$$a(x) = \sqrt{x} \quad (30)$$

Preprints (www.preprints.org) | NOT PEER-REVIEWED | Posted: 18 January 2021 doi:10.20944/preprints202101.0336.v1

$$a(x) = x^{0.414} \tag{31}$$

$$a(x) = \sqrt{1-(1-x)^{1.02}} \tag{32}$$

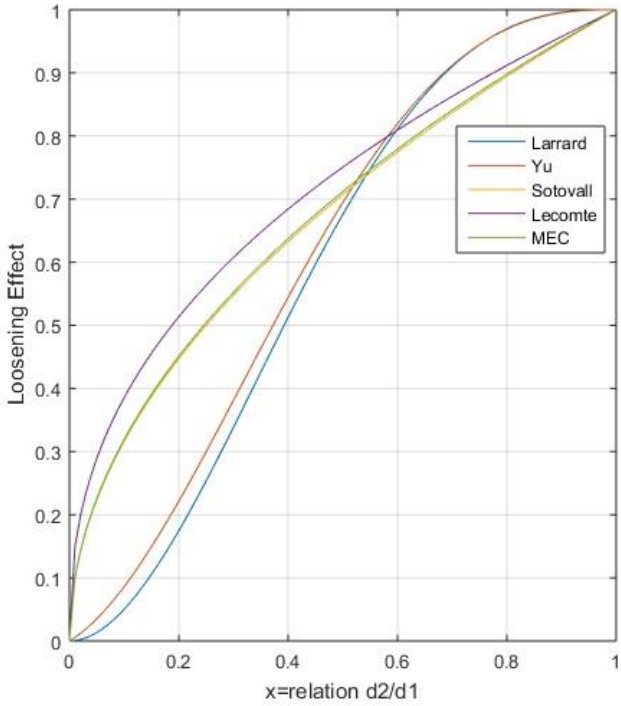

Figure 7. Loosening coefficient functions.

3. Effect of hydration of nanoadditions

It is clear that the process of establishing a high compactness in the granular skeleton is a guarantee in obtaining a high resistance of UHPC. In addition to this, the hydration products formed by the addition of nanoadditions also lead to an increase in strength that does not depend on the degree of compactness, [8, 43]. When cement is hydrated without additives this only occurs at the surface of the grain, meaning that the hydrated products grow and settle around it. This process prevents or reduces the ion transfer between the unhydrated cement particles and the surrounding solution, limiting the formation of a denser matrix of C-S-H [8]. The use of nanosilica will, in addition to increasing the degree of compactness, produce an early pozzolanic reaction on the silica surface and the creation of larger C-S-H gel layers andhigher crystallisation which will lead to a less porous network and more resistant concrete. Low percentages of nanosilica (some published authors suggest less than 2%,) have been shown to provide high values of resistance. In this work it has been observed that 1.5% of nanosilica in the presence of other additionsdoes not lead to a significant increase of the concrete strength. Nevertheless, a high content of nanosilica (close to 5%) creates a greater network of C-S-H, with nanosilica conferring greater viscosity to the paste that can trap air in the system and increase porosity. Studies by Yu *et al.*[8] showed that values higher than 4% of nanosilica caused an increase in the porosity of UHPC. The use of metakaolin affects the hydration kinetics and, for certain percentages of metakaolin, a greater quantity of C-S-H is obtained [44]. In the Kunther *et al*. research on the hydration kinetics of cements with different percentages of metakaolin substitution, the authors obtained an initial increase in the amount of C-S-H phases and a decrease in the portlandite content, accompanied by an increase in the amounts of calcium

Preprints (www.preprints.org) | NOT PEER-REVIEWED | Posted: 18 January 2021 doi:10.20944/preprints202101.0336.v1

aluminate hydrate phases. This increase in the C-S-H phase was also obtained with the joint use of nanosilica and metacaolin at 90 days in cement pastes in research carried out by Silva Andrade *et al*. [45] Therefore, there was a synergistic effect in the use of the two additions. The packaging models did not consider the optimal percentages as a function of hydration, which should always be present, as indicated above.

4. Results

Initially, three aggregates with sizes S_3 (0.5-1.6 mm), S_2 (0-1 mm), S_1 (0-0.5 mm) were used in the design of the granular skeleton. Experimental compactness, dry compactness and *Ci* of these aggregates were determined, with a compaction index of K=9 that provided values of c_{S3}=0.57, c_{S2}=0.62 and c_{S1}=0.56. The method used is that provided in the LPC test no. 61 [16], with the variation through vibration being that indicated by Sedran [17]. By means of the MEC, the maximum compactness reached was analysed as a function of the percentage of each aggregate. The greater degree of compactness was obtained in the mixture of aggregates S_3-S_1 with 60% of aggregate S_3, obtaining a compactness $\phi_{S3\text{-}S1}$=0.70. For a better understanding of this procedure, see Figure 8, Figure 9 and Figure 10.

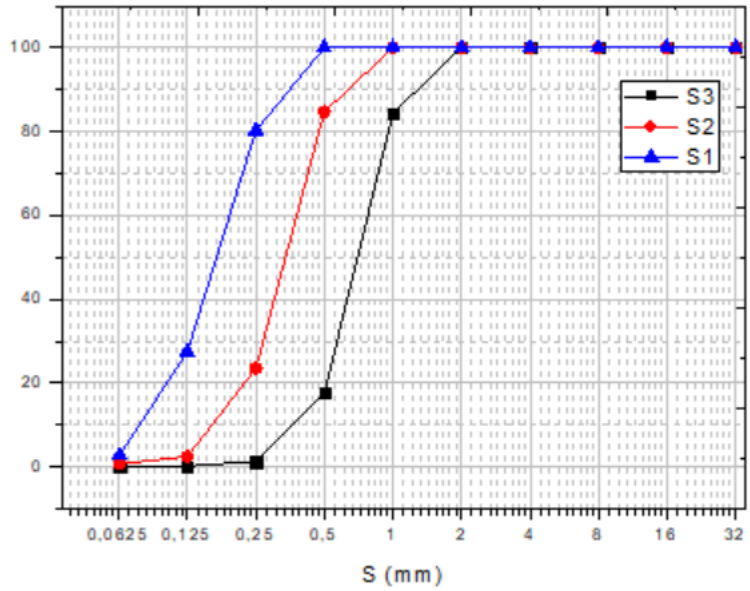

Figure 8 % Passage of the aggregates used.

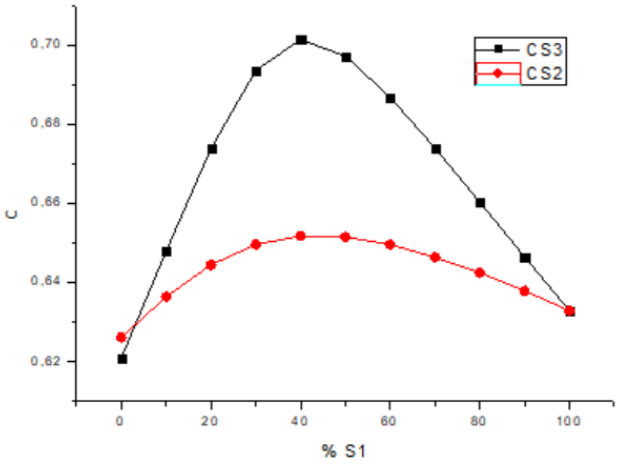

Preprints (www.preprints.org) | NOT PEER-REVIEWED | Posted: 18 January 2021 doi:10.20944/preprints202101.0336.v1

Figure 9 Aggregate compactness S_3-S_1, S_2-S_1.

In order to increase compactness, additions with sizes lower than 100 μm were used (including cement). The additions used in the models were limestone filler, metacaolin, silica fume and nanosilica.

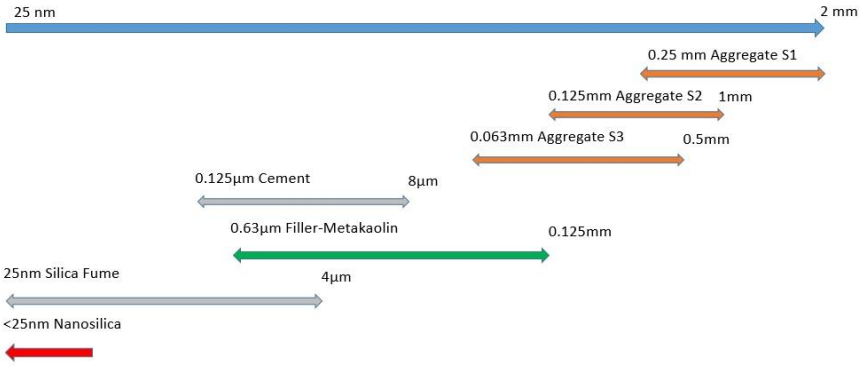

Figure 10. Size of aggregates and additions used.

In order to identify the compactness of these materials, the water demand test (K=6.7) and wet compactness (in accordance with standard EN 196-3 [19] and Sedran studies [41]) were used to compute expression (33), where c is the compactness, m_{H20} is the mass of water used, ρ is the density of the sample after drying and m is the dry mass.

$$c = \frac{1}{1 + \rho \cdot \frac{m_{H2O}}{m}} \tag{33}$$

Such a test is required to consider the dispersing or deflocculating effect of the additives which lead to an increase or change in the compactness of the tested material [17, 18]. The additive used was a high-performance superplasticizer Sika® ViscoCrete®-20 HE. The consequent additive ratio was established up to the saturation point of the additive, determined by means of a Marsh cone according to ASTM C-939 [29]. The flow time, and therefore the saturation point, varied depending on the addition used. The flow times of CEM I 52.5 R and of the silica fume cement slurry were determined in order to examine variation with and without addition, extrapolated to the behaviour with other additions. The results obtained indicated, for 100% cement, that the saturation point is established at 1.2% in weight of additive for the mixture of 80% cement and 20% silica fume and the saturation point at 3% in weight of additive. This can be observed in Figure 10.

Preprints (www.preprints.org) | NOT PEER-REVIEWED | Posted: 18 January 2021 doi:10.20944/preprints202101.0336.v1

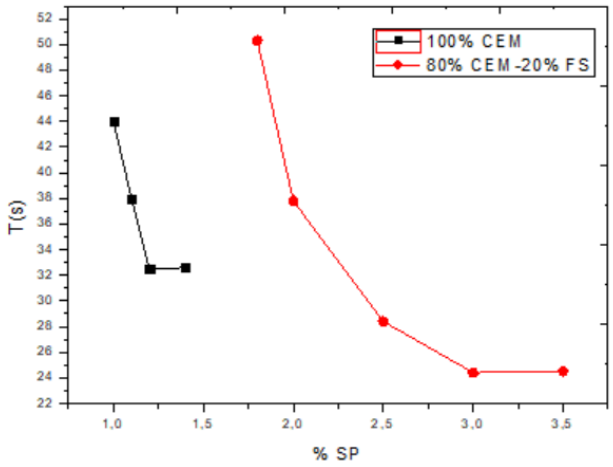

Figure 10. Saturation point of additive.

Once the saturation points of the additive have been determined, the wet compactness tests are carried out, verifying the variation of compactness with the percentage of additive. Thus, for filler and metakaolin, maximum values of compactness are obtained as $c_{FILL} = 0.64$, $c_{FILL} = 0.63$ for nanosilica and cement values of $c_{cem} = 0.62$, $c_{NS}=0.55$ for percentages in weight of additive of 1.2%. Silica fume compactness was $c_{SF} = 0.60$ with 3% wt. of superplasticizer additive. Figure 11 shows the experimental compactness of additions according to % of additive.

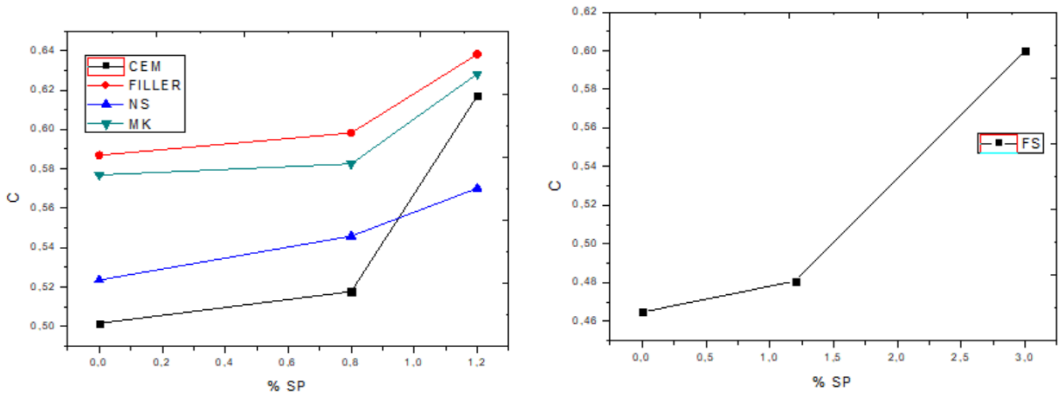

(a) *(b)*

Figure 11. Experimental compactness of additions according to % of additive.

Designs were established with the sand S_3 and sand S_1 and with a maximum of three additions. The percentage in volume of cement was established at between 35.2% and 43.3%. The compaction index was established at K=6.45 that was slightly lower than the wet compactness value and close to the K=6,7-7 value used in self-compacting concrete [17]. The maximum compactness was obtained with the combination of three additions and nano additions, filler or metakaolin+silica fume+nanosilica (starting with value five in Table 3). The maximum compactness value, ϕ=0.7899, is obtained with the combination of filler+silica fume+nanosilica, a value that was close to that achieved with the mixture of metakaolin+silica fume+nanosilica (ϕ=0.7881) with both mixtures having the same cement content.

Preprints (www.preprints.org) | NOT PEER-REVIEWED | Posted: 18 January 2021 doi:10.20944/preprints202101.0336.v1

Table 3. Compaction obtained according to model compressible packing.

Mix	Aggreg 1 (S_3)	Aggreg 3 (S_1)	Cement	Filler Limestone	Metakaolin	Sílica F.	nSi	ϕ
1	34.1	22.7	35.2	4		4	0	0.7750
2	34.1	22.7	35.2	4		4	0	0.7750
3	34.1	22.7	35.2	4		4	0	0.7750
5	27.1	18	43.3	4.1		4.2	3.3	0.7899
6	27.1	18	43.3	4.1		4.2	3.3	0.7899
7	27.1	18	43.3	4.2		4.2	3.2	0.7890
8	27.1	17.9	43.3	5.7		4	2	0.7870
9	27.1	19.6	43.3		4	4	2	0.7881

As indicated, the packaging models are not enough to obtain the results and properties sought in UHPC. The search for maximum compactness is not a guarantee of success. It is necessary to carry out an adequate combination in the additions in order to make the hydration complete, since the improvement of the additives allows a reduction of the *w/c* ratio up to values of 0.18. Studies by authors such as Rong, Xiao and Wang [31], verified the effect of silica fume on the hydration processes and microstructure of UHPC concrete, concluding that at low water/binder ratios silica fume dominated the hydration processes. Rong *et al*.[30] carried out the replacement of cement percentages by silica fume in UHPC mixtures. The researchers concluded that percentages of up to 3% of silica fume content led to an increase of compressive and flexural strengths of UHPC. Higher values create the opposite effect, due to an agglomeration of silica fume particles. The addition of nanosilica in percentages of up to 4% by weight of SiO2 cement accelerates the formation of C-S-H compounds, obtaining higher strengths at all ages [32], [33]; [34]. Land and Stephan [46] determined that there was an increase in the heat of hydration with the increase of the surface area. With percentages of between 3% and 5% in weight, increases in compressive strength of between 14% and 17% have been obtained with a decrease in the permeability of the concrete. Other authors, such as Brouwers *et al*.[9] and Yu *et al*. [10] have established values of up to 3.76% in nSi as optimal values for the improvement of mechanical properties. However, Senff *et al*.[37] did not obtain large increases in the compressive strengths of mortars and pastes with the addition of nanoparticles (SiO2 and TiO2), though they did obtain changes in rheology with increases in plastic viscosity. Authors such as Oertel *et al*. [35] obtained an increase in compressive strength at ages more than seven days with the addition of nSi in UHPC, though no clear relationship was established between the level of packing acquired, hydration and development of microstructure in the mixtures and the expected strengths. The use of metakaolin improves the workability times of the concrete and also needs a lower level of quantity of superplasticizer to obtain the same consistency. Tafraoui *et al*. [38] obtained an improvement in the bending strength of UHPC treated at 90 ºC and 150 ºC. However, El Gamal *et al*. [39] made mixtures combining metakaolin and silica fume with improved results in resistance than using only metakaolin. Morsy *et al*. [40] obtained increases in flexural strength in mortars mixed with metakaolin (up to 7.5% in weight of mixture) and silica fume that only with the addition of the latter for pastes with the same *w/c* ratio, between 7.5% and 10% of the strength decreased.

Table 4 shows the % by volume of the components of each mixture, as well as the compaction index and compactness obtained.

Preprints (www.preprints.org) | NOT PEER-REVIEWED | Posted: 18 January 2021 doi:10.20944/preprints202101.0336.v1

Tabla 4 Components of each mixture, compaction index and compactness.

Mix	1	2	3	5	6	7	8	9
ϕ	0.7750	0.7750	0.7750	0.7899	0.7899	0.7890	0.7870	0.7881
K	6.45	6.45	6.45	6.45	6.45	6.45	6.45	6.45
Aggreg 1 S_3	27.2	27.2	27.2	20.7	20.7	20.7	20.6	21.5
Aggreg 3 S_1	18.1	18.1	18.1	13.8	13.8	13.8	13.8	14.3
Cement	28.0	28.0	28.0	33.2	33.2	33.2	33.2	33.2
Fíller	3.2	3.2	3.2	3.2	3.2	3.2	4.5	
Sílica F	3.2	3.2	3.2	3.2	3.2	3.3	3.1	3.1
Metakaolín								3.1
nSi				2.5	2.5	2.4	1.5	1.5
Air	2	2	2	2	2	2	2	2
Water	16	16	16	19	19	19	19	19
Additive SP	2.3	2.3	2.3	2.3	2.3	2.3	2.3	2.3

Table 5 sets out the results of the mixing times with w/c=0.18. The mixing times increased with the number of additions. Mixtures 1-3 had equal times, with the same occurring with mixtures 5-7. Mixture 8 had a longer mixing time than mixtures with the same number of additions, due to the increase in filler content even though there was a reduction in silica and nanosilica fume content. Mixture 9, with the same silica and nano-silica fume content as Mixture 8, experienced a reduction in mixing time as it was designed with metakaolin instead of filler.

Table 5 Mixing-time results.

Mix	Mixing time (s)
1	270.0
2	270.0
3	270.0
5	300.0
6	300.0
7	300.0
8	540.0
9	480.0

Figure 12 shows the electric intensity experienced by the engine of the mixer during the mixing process, compared with the elapsed time. This allows an indirect measure of the consistency of the concrete to be established. In addition to setting the most appropriate mixing times, in this figure, the mixing times and engine intensity have been transferred for a mixture with two additions, Mixture 1, and with three additions, Mixture 5. This analysis should be carried out with the same mixer and with the same volume of mix. The intensity vs. mixing-time curve is usually divided into three zones. In the first zone, the curve experiences an increase in intensity vs. time given that in such a time the additive and the mixing water do not produce a substantial modification of the rheology of the mixture. In the second zone, the curve has an inflection point where the intensity is maximum, from which such intensity is reduced beacause the additive and the mixing water modify the rheology of the mixture, making it more fluid. The third zone of the curve tends

Preprints (www.preprints.org) | NOT PEER-REVIEWED | Posted: 18 January 2021 doi:10.20944/preprints202101.0336.v1

to be horizontal, obtaining the maximum fluidity of the mixture and determining the mixing time. It can be seen that Mixture 5 has a higher peak intensity than Mixture 1 due to the greater number of additions, which makes it more difficult for the additive and the water to modify the rheology, although this occurs earlier than in Mixture 1. The second and third zones are similar across the two mixtures, with Mixture 5 taking a few seconds more than Mixture 1.

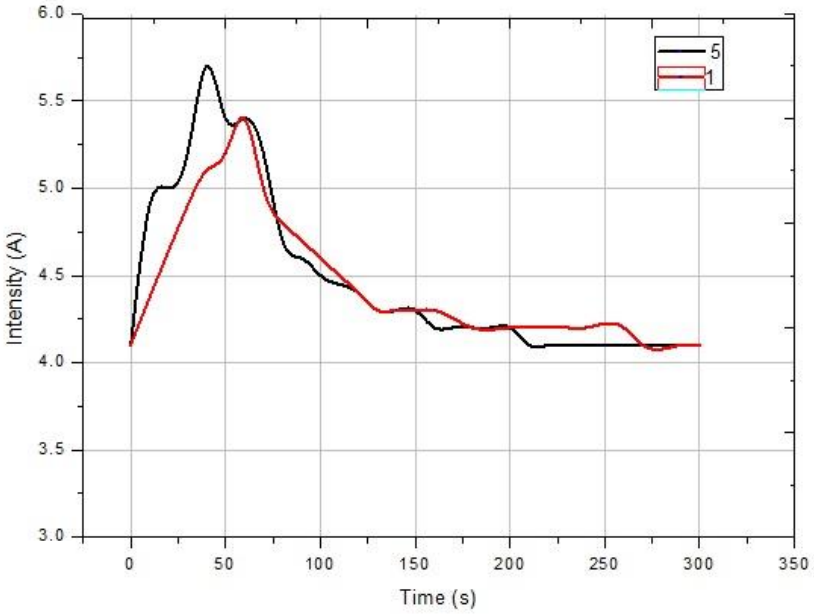

Figure 12. Intensity of electricity vs time of mixing

The following are the results obtained for compressive strength in a cubic specimen. For mixtures 1-3 with two additions, with the same cement content and compactness, a seven-day average strength of 8.7 MPa and a deviation of 3.45 MPa I was obtained. At 28 days the average strength obtained was 119.5 MPa with a greater deviation of 4.42 MPa. Mixtures 5-9 were made with the same percentage of cement, higher than that used in mixtures 1-3 and three additions. With different values of compactness, though higher than those obtained with two additions, mixtures 5-6 exhibited lower compression resistance values than mixtures 7-9, even though they were more compact (even mixture 6 experienced a drop in resistance at 28 days compared with seven days). If mixture is compared with mixture 7 and mixture 9, it is clear that the metakaolin used confers a greater resistance to compression with less compactness.

Table 6 Compressive strength at s and 28 days.

Mixture	ϕ	R7 cub (MPa)	R28 cub (MPa)
1	0.7750	81.3	117.0
2	0.7750	80.1	124.6
3	0.7750	86.6	116.9
5	0.7899	91.7	89.7
6	0.7899	83.0	97.3
7	0.7890	93.7	121.7
8	0.7870	96.8	101.5
9	0.7881	89.3	121.1

Preprints (www.preprints.org) | NOT PEER-REVIEWED | Posted: 18 January 2021 doi:10.20944/preprints202101.0336.v1

Figure 13 sets out the results provide in the table above. By analysing the results of the group of mixtures 1-3 with two additions, with a lower cement content and less compactness than the group of mixtures 5-9 with three additions, with a higher cement content and greater compactness, it may be determined that greater compactness in the mixture does not lead to greater strength, although mixtures with greater compactness may have a greater durability.

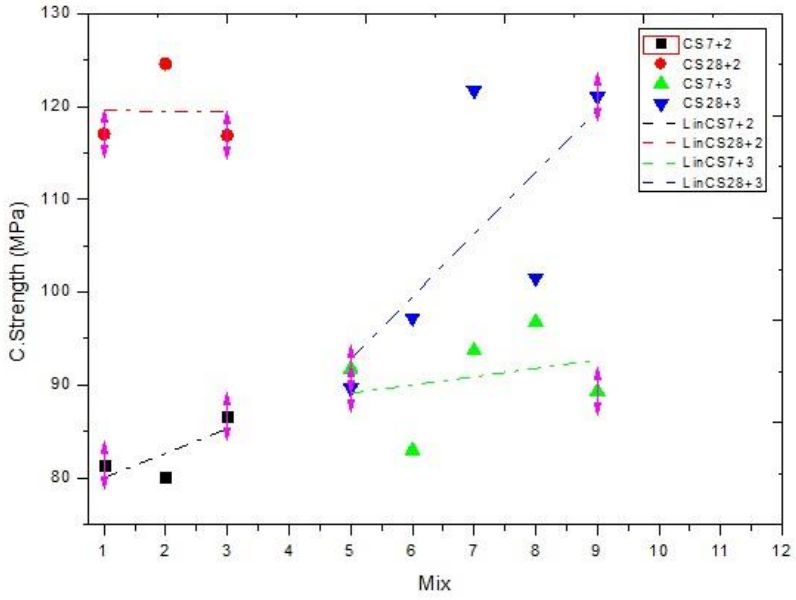

Figure 13. Compressive strength results

Figure 14 compares the compression strength at seven and 28 days with the compactness obtained. At seven days, there is a direct proportional relationship between compactness and strength achieved, also considering that the mixes with greater compactness have a higher cement content. However, this relationship is reversed with the results at 28 days, with higher compressive strengths being obtained in mixes with two additions (with less compactness and lower cement content).

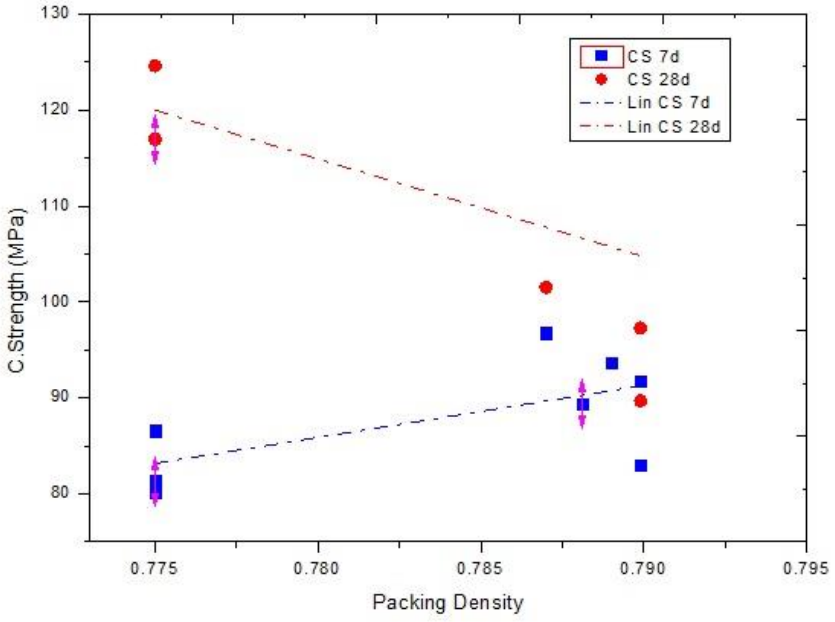

 doi:10.20944/preprints202101.0336.v1

Figure 14. Compressive strength results according to compactness.

This article has analysed the packaging models from their beginnings and evolution to the most developed models. Initially, continuous models, such as those offered by Fuller and Thompson, sought to achieve a theoretical curve or parabola by relating the size of particles to their maximum size. The development of these models was centred on the variation of the parabola parameter (Gessner's parameter and modifications made to it by Andreasen and Andersen [7]). In addition, the relation with the minimum size, allowing a greater compactness of the mixtures but not permitting an adequate response when using particles smaller than 250 μm taken into account. The need to establish greater compactness in sectors other than concrete leads to the appearance of discrete models, initially binary, such as that provided by Furnas which would evolve into multi-component models where the relationship between particles of different sizes in a given mixture could be established. Later, with the studies carried out by Ben-Aïm, Sotovall and De Larrard *et al*., based on previous works by Caquot and Mooney, the wall and loosening effects that occur in the mixture of particles of different sizes and their environment are established which affect the compactness of the bulk material. Later, De Larrard also established the relationship between virtual and real compactness according to the method and index of compaction to which the mixture is subjected. The degree of compactness can be determined according to the external conditions of placement. These models make it possible to obtain multi-component mixtures independently of their size. The need to search for a high-degree packing in the UHPC makes these models the most relevant ones. The development of additives that allow the addition of water to be necessary for hydration of the particles makes such models more significant in the field of concrete. However, in addition to maximum compactness, the hydration conditions of the compounds and the contribution to the fresh and hardened states should be considered. Therefore, a design is required to respond not only to the acquisition of maximum compactness of the solid components but also the appropriate proportions of those solids regarding hydration and activity. Thus, in mixtures with a lower content of additions, lower cement content and less compactness, higher compressive strength values are obtained than in mixtures with a greater number of additions, cement content and compactness. However, the latter are expected to provide the concrete with greater durability. This was verified in mortars examined by Alonso Dominguez *et al*. [42] where the use of nanoadditions such as nanosilica allowed a porous network with a smaller pore diameter to be obtained. This led to an improvement in electrical resistivity and chloride migration coefficients, thus providing the mortars with greater durability, although these studies were not carried out with as great an amount of cement content and such a low *w/c* ratio.

4. Conclusions

1) A dosification of UHPC by means of packaging models in combination with the assessment of the activity of nanoadditions in the hydration processes of cement is a promising way for improving the design of UHPC. The maximum compactness of the particles, when nanoadditions are used, does not always obtain the best resistance and durability of the UHPC. Consideration of the role of nano-additions in gaining resistance and durability properties is a key aspect.

2) The highest compactness, of the three sands used, was obtained with the use of two of them (the thickest S_3 and S_1 with 60% of aggregate S_3 that obtained, through De Larrard's packaging model, a compactness of $\phi_{S3\text{-}S1}$=0.70. The compactness was unaffected by the use of an intermediate sand S_2

3) The use of nanoaditions of various sizes permits an increase, through use of the same model, in the conmpactness of the mixtures. The higher degree of compactness was

achieved by using three additions: limestone filler, silica fume and nanosilica (ϕ=0.7899).

4) The measurements of the mixing times, by using the amperimeter of the mixer, were always longer for the mixes with three nanoadditions than for ones with two nano additions for the same percentages of additive.

5) The designs made with three additions and higher cement content led to better compressive strengths at seven days than those designs made with two additions and a lower cement content. The presence of nanoadditions, such as nanosilica, improved C-S-H gel formation and thus better results at earlier ages.

6) The compressive strength results at 28 days of mixtures with two additions were good and even higher than those obtained with mixtures with three additions, in spite of exhibiting a lower compactness and cement content. A higher percentage of nano-addition in the mixture may be and inadequate and lead to the opposite effect.

7) The mixture with additions of metakaolin and nanosilica, with the latter showing slightly lower percentages than other mixtures with three additions 1.5% in volume, allows higher compressive strengths than the use of nanosílice alone to be obtained. The synergy in the use of both components is demonstrated.

6. Acknowledgements

The authors gratefully acknowledge the financial support provided by Ministry of Economy and Competitiveness of Spain by means of the Research Fund Project PID2019-108978RB-C31. They also offer their gratitude to SIKA SAU and Calle 30 for supporting the Enterprises University Chairs “Cátedra Sika-UPM” and “Cátedra Universidad Empresa Calle30-UPM” respectively.

References

[1] FHWA-HRT-13-060, «Ultra-High Performance Concrete: A State-of-the-Art Report for the Bridge Community,» Federal Highway Administration, 2013.

[2] A. Naaman and K. Wille, «Some Correlation Between High Packing Density, Ultra-High,» de *2º Congresso Ibérico sobre betão auto-compactável*, Guimaraes, 2010.

[3] T. Teichmann and M. Schmidt, «Influence of the packing density of fine particles on structure, strength and durability of UHPC,» de *International Symposium on Ultra High Performance Concrete*, Kassel (Alemania), 2004.

[4] D. Cumberland and R. Crawford , The Packing of Particles, Elsiever, 1987.

[5] Y. Konakawa and K. Ishizaki, «The particle size distribution for the highest relative density in a compacted body,» *Powder Technology,* pp. 241-246, 1990.

[6] P. Grinspan, «Interpretación y medición comparada de líneas granulométricas continuas,» *Materiales de Construcción. CSIC,* pp. 37-47, 1979.

[7] A. Andreasen and J. Andersen, «Ueber die Beziehung zwischen Kornabstufung und Zwischenraum in Produkten aus losen Körnern (mit einigen Experimenten),» *Kolloid-Zeitschrif,* pp. 217-228, 1930.

[8] R. Yu, P. Spiesz and H. Brouwers, «Effect of nano-silica on the hydration and microstructure development of Ultra-High Performance Concrete (UHPC) with a low binder amount,» *Construction and Building Materials*, pp. 140-150, 2015.

[9] H. Brouwers and H. Radix , «Self-compacting concrete: the role of the particle size distribution,» First International Symposium on Design, Performance and Use of Self-Consolidating Concrete, Changsha, Hunan, (China), 2005.

[10] R. Yu, P. Spiesz and H. Brouwers, «Mix design and properties assessment of Ultra-High Performance Fibre Reinforced Concrete (UHPFRC),» *Cement and Concrete Research*, pp. 29-39, 2014.

[11] A. Espinoza, «Estudio de dosificación de hormigón de ultra alta resistencia, basada en el empaquetamiento de los áridos,» TFM Universidad Politécnica de Madrid, 2010.

[12] H. Masuda , K. Higashitani and H. Yoshida, Powder technology. Fundamentals of particles, powder beds and particle generation, Boca Raton (USA): CRP Press, 2006.

[13] S. Liu and Z. Ha, «Prediction of random packing limit for multimodal particle mixtures,» *Powder Technology*, p. 283–296, 2002.

[14] G. Roquier, «Etude de la compacité optimale des mélanges granulaires binaires: classe granulaire dominante, e de paroi, de desserrement,» T.D. Université Paris-Est, 2014.

[15] T. Sedran and F. De Larrard, «Optimization of ultra hight performance concrete by using a packing model,» de *Cement and Concrete Research vol 24*, 1994, pp. 997-1009.

[16] LPC, «LPC Nº 61 Essai de compacité des fractions granulaires,» LCPC, Paris (Francia), 2004.

[17] T. Sedran, «Rheologie et rheometrie des betons. application aux betons autonivelants,» T.D. L'ecole nationale des pontos et chaussees, Paris (Francia), 1999.

[18] S. Formagini, Dosagem Científica e Caracterizaçao Mecânica de Concretos de Altíssimo Desempenho, Rio de Janeiro: Universidade Federal do Rio de Janeiro , 2005.

[19] EN 196-3 «Methods of testing cement - Part 3: Determination of setting times and soundness» 2017.

[20] J. Funk and D. Dinger, Predictive Process Control of Crowded Particulate Suspension, Applied to Ceramic Manufacturing, Kluwer Academic Press, 1994.

[21] O. Koutný,[1] J. Kratochvíl, J. Švec and J. Bednárek, «Modelling of packing density for particle composites design,» de *International Conference on Ecology and new Building materials and products, ICEBMP* , Černá Hora (Czech Republic), 2016.

[22] R. Ben-Aïm, «Étude de la texture des empilements de grains. Application à la détermination de la perméabilité des mélanges binaires en régime moléculaire, intermédiaire,laminaire.,» T.D. 'Université de Nancy., 1970.

[23] T. Stovall, F. De Larrard and M. Buil, «Linear Packing Density Model Grain Mixtures,» *Powder Technology,* pp. 1-12, 1986.

[24] M. Mooney, «The viscosity of a concentrated suspension of spherical particles,» *J.Colloid Sci,6, 162,* 1950.

[25] A. Yu and N. Standish, «An Analytical-Parametric Theory of the Random Packing of Particles,» *Powder Technology,* pp. 171-186, 1988.

[26] F. De Larrard, Structures granulaires et formulation des bétons, Nantes (Francia): LCPC, 1999.

[27] F. De Larrard, «Formulation et propriétés des bétons à très hautes performances,» *Rapport de recherche LPC n°149,* 1988.

[28] A. Yu, R. Zou y N. Standish, «Modifying the linear packing model for predicting the porosity of nonspherical particle mixtures,» *Industrial & Engineering Chemistry Research 35,* pp. 3730-3741, 1996.

[29] C. ASTM, «ASTM C939 Standard Test Method for Flow of Grout for Preplaced-Aggregate Concrete (Flow Cone Method),» ASTM, 2002.

[30] Z. Rong, W. Sun, H. Xiao and G. Jian, «Effects of Nano-SiO2 Particles on the Mechanical and Microstructural Properties of Ultra-high Performance Cementitious Composites,» *Cement and Concrete Composite,* pp. 25-31, 2015.

[31] Z. Rong, W. Sun, H. Xiao and W. Wang, «Effect of Silica Fume and Fly Ash on Hydration and Microstructure Evolution of Cement Based Composites at Low Water–binder Ratios,» *Construction and Building Materials,* pp. 446-450, 2014.

[32] A. Nazari and S. Riahi, «The effects of SiO2 nanoparticles on physical and mechanical properties of high strength compacting concrete,» *Composites Part B: Engineering* , p. 570–578, 2011.

[33] H. Jennings , J. Chen and J. Thomas, «Influence of Nucleation Seeding on the Hydration Mechanisms of Tricalcium Silicate and Cement,» *The Journal OF Chemical Chemistry,* p. 4327–4334, 2009.

[34] H. Romero, J. Gálvez, I. Lucea y A. Moragues , «Durabilidad y propiedades mecánicas del hormigón autocompactante con adición de microsílice y nanosílice,» 3º Congreso Iberoamericano sobre hormigón autocompactante, 2012.

[35] F. Huttera, R. Tänzer and T. Oertel, «Primary particle size and agglomerate size effects of amorphous silica in ultra-high performance concrete,» *Cement and Concrete Composites,* pp. 61-67, 2013.

[36] H. Li, H. Xiao, J. Yuan and J. Ou, «Microstructure of cement mortar with nano-particles,» *Composites Part B: Engineering,* p. 185–189, 2004.

[37] L. Senff, D. Hotzab, S. Lucasc and V. Ferre, «Effect of nano-SiO2 and nano-TiO2 addition on the rheological behavior and the hardened properties of cement mortars,» *Materials Science and Engineering,* p. 354–361, 2012.

[38] A. Tafraoui, G. Escadeillas , L. Soltane and T. Vidal, «Metakaolin in the formulation of UHPC,» *Construction and Building Materials,* p. 669–674, 2009.

[39] S. El-Gamal, M. Amin and M. Ramadan, «Hydration characteristics and compressive strength of hardened cement pastes containing nano-metakaolin,» *HBRC Journal,* pp. 114-121, 2014.

[40] M. Morsy, Y. Al-Salloum, T. Almusallam and H. Abbas, «Effect of nano-metakaolin addition on the hydration characteristics of fly ash blended cement mortar,» *Journal of Thermal Analysis and Calorimetry* , pp. 845-852, 2013.

[41] T. Sedran, F. De Larrard et L. Le Guen, «Determintion de la compacité des ciments et additions minerales a la sonda de Vicat,» *Note technique LCPC Nantes.*

[42] D. Alonso-Domínguez, I. Álvarez-Serrano, E. Reyes and A. Moragues, «New mortars fabricated by electrostatic dry deposition of nano and microsilica additions: Enhanced properties,» *Construction and Building Materials,* pp. 186-193, 2017.

[43] S. Haruehansapong, T. Pulngern and S. Chucheepsakul, «Effect of the particle size of nanosilica on the compressive strength and the optimum replacement content of cement mortar containing nano SiO2,» *Construction and Building Materials,* p. 471–477, 2014.

[44] W. Kunther, Z. Dai and J. kibsted, «Thermodynamic modeling of hydrated white Portland cement–metakaolin–limestone blends utilizing hydration kinetics from 29Si MAS NMR spectroscopy,» *Cement and Concrete Research,* pp. 29-41, 2016.

[45] D. da Silva Andrade, J. H. da Silva Rêgo, P. C. Morais and M. Frías Rojas, «Chemical and mechanical characterization of ternary cement pastes containing metakaolin and nanosilica,» *Construction and Building Materials,* pp. 18-26, 2018.

[46] L. Gerrit y S. Dietmar, «Controlling cement hydration with nanoparticles,» Cement & Concrete Composites, nº 57, pp. 64-67, 2014